Astron. Astrophys. 340, 287–299 (1998)

ASTRONOMY AND ASTROPHYSICS

On the steady state of nonlinear quasiresonant Alfvén oscillations in one-dimensional magnetic cavity

Luigi Nocera[1] **and Michael S. Ruderman**[2,3]

[1] Institute of Atomic and Molecular Physics, National Research Council, Via Giardino 7, I-56127 Pisa, Italy
[2] School of Mathematical and Computational Sciences, St Andrews University, St Andrews, Fife KY16 9SS, Scotland, UK
[3] On leave of Institute for Problems in Mechanics, Russian Academy of Sciences, Vernadskii Prosp. 101, 117526 Moscow, Russia

Received 7 May 1998 / Accepted 21 September 1998

Abstract. We study the steady state of nonlinear, small-amplitude, quasiresonant Alfvén oscillations in a homogeneous dissipative hydromagnetic cavity which is forced by the shear motion of its boundaries. It is shown that, even in the case of strong nonlinearity, these oscillations can be represented, to leading order, by a sum of two solutions in the form of oppositely propagating waves with permanent shapes. An infinite set of nonlinear equations for the Fourier coefficients of these solutions is derived which, in general, admits multiple solutions, depending on the re-scaled total Reynolds number, R, and mistuning, Δ, between the frequency of the boundary forcing and the first Alfvén eigenmode of the cavity. Two types of solutions are found. On the one hand, *low-modal* solutions set in over the entire parameter range studied, which can be represented, with a remarkable accuracy, by very few Fourier modes even at very large R. For a fixed Δ the time-averaged energy, $\mathcal{E}$, that can be stored in the cavity is saturated, as R increases, to a value which is approximately proportional to ϵ^2, $\epsilon^3 \ll 1$ being the Alfvén Mach number of the boundary motions. The time-averaged absorbed power (the Poynting flux $\mathcal{S}$) scales as $1/R$. For suitable values of R and Δ catastrophic transitions occur between these solutions, in which the average power released scales as R, provided $R < \epsilon^{-1/2}$. The second type of solutions sets in for a narrow window of Δ and develops *large gradients* (shocks) which need to be represented by many Fourier modes. For a fixed Δ the build-up of these gradients takes place starting from a low-modal solution in either a continuous way, by increasing R, or in a sudden catastrophic way as R becomes smaller than a critical value. *Both* $\mathcal{E}$ and $\mathcal{S}$ are saturated as R is increased. It is suggested that both types of solutions can explain bright events in the solar atmosphere.

Key words: MHD – waves – Sun: chromosphere – Sun: corona – Sun: oscillations

1. Introduction

Recent ground-based and space observations have revealed a complex scenario of solar atmospheric oscillations in which the wave fields in the photosphere, sunspots, chromosphere, transition region and finally in the corona are intricately interconnected (Ulmschneider et al. 1991; Zirin et al. 1991). Data from the SOHO mission (e.g. Judge et al. 1997) support the idea that even the quiet Sun's chromosphere is a very dynamic medium. In particular, a few open questions have been attracting special attention which may have an explanation within the framework of wave dynamics, i.e. chromospheric and coronal heating and bright points. Related areas, such as waves in the umbrae of sunspots (e.g. Lites 1992), p-modes in photospheric cavities (e.g. Duvall et al. 1993), coronal heating by both linear (Ionson 1978; Kuperus et al. 1981; Davila 1987; Hollweg 1990; Goossens 1991; Ruderman et al. 1997) and nonlinear (Ofman et al. 1994; Ofman & Davila 1995; Tirry & Poedts 1998) resonance absorption, spicules (Cargill et al. 1997) and transition region UV bursts (Bocchialini et al. 1997) are also receiving much attention in the solar physics community.

Ca II bright grains occurring in the network cell interior are traditionally explained as a purely radiative hydrodynamic phenomenon (Remling et al. 1996). By the integration of the full 1D hydrodynamic and non-LTE radiative transfer equations, Carlsson & Stein (1997) arrive at the conclusion that bright grains are produced primarily by waves propagating from the photosphere and eventually steepening into shocks. They also note the role of wave interference in modifying the time distribution of bright points. This idea has also been suggested by Hofman et al. (1996) who observe a high horizontal mobility of the bright grains and ascribe them to constructive interference of p-modes propagating in the chromosphere (see also Steffens et al. 1996a).

The shock mechanism has encountered some criticism on the grounds that the abundant shock production by the simulation does not match the observed low contribution of grains to the overall emission (Steffens et al. 1996a). Another criticism concerns the nature of the 'piston' driver which would excite the waves and eventually cause bright events and which Carlsson and Stein (1997) locate at a height of $\simeq 260\,\mathrm{km}$ by matching the Fe I observations by Lites et al. (1993): according to this criticism, the detailed reproduction of the observed $\mathrm{Ca\ II\ H}_{2V}$ time series suggests only a strong correlation between the Fe I and the Ca II layers rather than the existence of a 'piston'.

Send offprint requests to: L. Nocera

The issue of the nature and location of the velocity fields which power chromospheric wave dynamics is in fact still controversial, possibly because long time series of highly resolved 2D spectrograms are still unaffordable. Some authors advocate an in-chromospheric source for the grains (Kneer & von Uexküll 1993). Others use the model of an external acoustic piston (e.g. Carlsson & Stein 1997; Cheng & Yi 1996; Schmitz & Fleck 1995; Theurer et al. 1997). However recent cross-correlation studies of different atmospheric layers suggest a poor connectivity between different chromospheric layers and cast some doubts about this model (e.g. Hoekzema & Rutten 1998). On the other hand, connectivity could be improved by the magnetic field, as shown, much deeper in the atmosphere, by a comparative study of the global modes at the minimum and near the maximum phase of the solar cycle (Foglizzo et al. 1998). Bocchialini et al. (1997) use SUMER to infer correlation between chromospheric (Ly_ϵ) and transition region (S VI) bright events. Carlsson et al. (1997) also study SUMER data and attribute a role to the magnetic field.

Other authors positively claim a role for the magnetic field in chromospheric dynamics. The study of the Ca II K line in a 2D magnetized atmosphere (Solanki et al. 1991) and of the Fe I and Fe II lines emerging from the strongly magnetized flux tubes associated with pores (Kneer et al. 1996; Ploner & Solanki 1997; Stolpe & Kneer 1997) suggests that a static magnetic field does have a role in determining chromospheric line shapes. Some authors suggest a high correlation of the intense bright points with the location of magnetic flux tubes on the cell boundary (Kalkofen 1997) and even in the cell interior (Kalkofen 1996; Sivaraman & Livingston 1982). By studying the photospheric Fe I lines Soltau (1997) concludes that Ca II K bright points are tracers for photospheric magnetic flux concentrations (knots). However, the conclusion by Sivaraman & Livingston (1982) that emission from the grain may contribute conspicuously to the integrated Ca II K line profile on account of the abundance of magnetic elements has not been confirmed by other authors. To overcome this inconsistency, Kalkofen (1996) postulates a *threshold* for the strength of the magnetic field in the flux tubes, below which bright points would not be lighted.

In both the radiative-hydrodynamic and the 'magnetic' scenarios the irregularity in both time behaviour and spatial distribution of these bright points is attributed to nonlinearity, a possibility advocated especially by von Uexküll & Kneer (1995).

Studies of chromospheric oscillations have also been pursued independently from the phenomenology of the grains. One example is the observation of 5.6 mHz oscillations in the chromosphere (Harvey et al. 1993) which has prompted some authors (Steffens et al. 1995; Deubner et al. 1996) to suggest the existence of cavities, although these have not yet been associated with an observed morphological counterpart. The idea of multiple modes in such cavities having distinct nodal planes is instrumental to explaining the spectroscopic properties of the NaD_2 line and it has been further developed to include a realistic model atmosphere (Steffens et al. 1996b).

Besides being important in its own right, the study of chromospheric oscillations is also relevant for the understanding of the spectrum of waves emerging at the base of the corona which, in wave theories, are assumed to heat the solar corona and to accelerate the solar wind. This applies to both recent theories based on high frequency (1Hz – 1kHz) Alfvén waves (Tu & Marsch 1997) and to the more conventional approaches based on the low frequency (mHz) band (Ulmschneider et al. 1991).

As a result of this broad range of investigations, the need has emerged for a nonlinear study of oscillation in the solar atmosphere, which is particularly important for Ca K bright points (von Uexküll & Kneer 1995). This paper is an attempt to put nonlinear effects in the perspective outlined above and to take into account the following basic facts:

i) the existence of cavities;
ii) the action of an external source coupled to the cavity's plasma;
iii) the existence of acoustic shocks;
iv) the existence of a threshold mechanism limiting the occurrence of bright events.

As discussed above, fact i) suggests that we rather give a role to the magnetic field, which we do by embedding the cavity in a uniform magnetic field. Fact iii) implies that we retain the acoustic (or rather magnetoucoustic) component of the wave field. Facts iii) and iv) imply nonlinear theory. Rather than attempting an *ab initio* integration of the MHD equations, we use numerical techniques to substantiate and update existing simple analytical models. We shall thus abide by a relatively simple 1D model, being comforted by the work by Carlsson & Stein (1997) who could produce a remarkable agreement with observation by an even 1D model.

As crude as this approach may appear, it proves to be fruitful when we investigate the *steady* rather than dynamic state of the oscillations. The idea is that key phenomena in the solar atmosphere can be interpreted as *structural instabilities* of these steady states: close to these instabilities (or *bifurcations*) the relevant dynamics of the oscillations may be approximated by simple (or *normal form*) equations. Such an approach will greatly reduce the numerical effort and will thus allow a more extensive exploration of the space of parameters which characterize the cavity.

We have thus outlined the main features of a *hydromagnetic cavity*. Hydromagnetic cavities – considered as dissipative systems open to external disturbances – provide a very convenient setting where the dynamics of MHD oscillations can be given a rigorous treatment. The structural instabilities studied so far include bistability (Nocera & Priest 1991), subharmonic sequences (Nocera 1994), homoclinic chaos (Nocera et al. 1997) and Hopf bifurcations (Bologna & Nocera 1998).

In this paper we shall thus study the steady state of nonlinear quasi-resonant driven Alfvén oscillations in a homogeneous magnetic cavity which is driven by the shear harmonic motion of one of its boundaries (the other one being kept fixed). Shear driving motions are rather unconventional in the models of chromospheric flux tubes, the acoustic piston being more popular. However, recent observations of the Fe I photospheric line have revealed an excess of horizontal over vertical motions

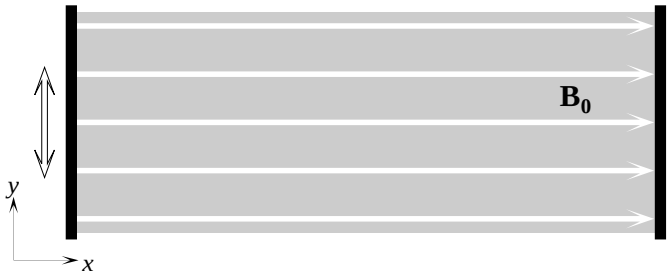

Fig. 1. Sketch of the cavity with one moving (*left*) and one fixed (*right*) boundary. The equilibrium pressure, p_0, density ρ_0, and magnetic field, $\mathbf{B}_0$, are homogeneous and constant in time.

(Volkmer et al. 1995). We show that the key parameter which governs the response of the cavity is the mismatch between the frequency of the boundary motion and the eigenfrequency of its first Alfvén eigenmode. Earlier, simple models of the oscillations based on the single-mode description of the cavity (Nocera & Priest 1991) turn out to hold remarkably well, except in a narrow range of this parameter. In particular, several branches of the steady state solution are possible: the structurally unstable ones bifurcate to the stable ones via saddle-node bifurcations as the driver's frequency is varied, thus producing multistability and hysteresis. Shocks will appear in the narrow parameter range where the single mode description is insufficient: bifurcations between non-shocked and shocked solutions take place as the second key parameter (the Reynolds number) is varied.

The paper is organized as follows. In the next section we give the setup of the problem and discuss main assumptions. In Sect. 3 we derive the governing equation for the nonlinear quasi-resonant driven Alfvén waves written in the form of an infinite set of algebraic equations for the Fourier coefficients. In Sect. 4 we derive expressions for the energy of Alfvén oscillations in the cavity and for the energy flux into the cavity. In Sect. 5 we consider the bifurcations of the system in the parameter range where multiple solutions exist. In Sect. 6 we study a particular range of parameters where solutions with very large spatial gradients (shocks) exist. In Sect. 7 we present the discussion of our results and conclusions.

2. Basic equations and assumptions

We consider a homogeneous hydromagnetic cavity with an equilibrium magnetic field in the x-direction (see Fig. 1). At one end of the cavity the plasma is at rest, while it is homogeneously driven in the y-direction at the other end. Throughout the cavity the z-components of the velocity and the magnetic field are zero, and perturbations of all quantities depend on x and t only.

The plasma is assumed to be viscous and resistive, viscosity and resistivity being isotropic. The last assumption is not satisfied for the solar corona where viscosity is strongly anisotropic. However in what follows we consider Alfvén oscillations only. Although we shall develop a nonlinear theory of such oscillations, dissipative terms in the momentum equation and in the induction equation are taken in the linearized form. In the case of Alfvén oscillations, the leading term in the linearized tensorial expression for viscosity (proportional to η_0, Braginskii 1965) is zero. This fact enables us to use isotropic viscosity in what follows. Furthermore, in the corona, the Hall term, which appears in the generalized Ohm's law due to anisotropy of electrical conductivity, is larger than the resistive term. However, we need non-ideal terms in the momentum and induction equations to provide dissipation only, whereas the Hall term in the induction equation provides dispersion. We thus neglect this term.

Let us introduce the viscous and magnetic Reynolds numbers

$$R_{\rm e} = \frac{LV_A}{\bar{\nu}}, \quad R_{\rm m} = \frac{LV_A}{\bar{\lambda}}, \tag{1}$$

where L is the length of the magnetic cavity, $\bar{\nu}$ kinematic coefficient of the shear viscosity, and $\bar{\lambda}$ coefficient of magnetic diffusion. The square of the Alfvén speed V_A is given by

$$V_A^2 = \frac{B_0^2}{\mu\rho_0}, \tag{2}$$

where B_0 is the equilibrium magnetic field, ρ_0 the equilibrium density, and μ the magnetic permeability. To characterise the total dissipation due to both viscosity and resistivity we introduce the total Reynolds number $R_{\rm t}$ given by

$$\frac{1}{R_{\rm t}} = \frac{1}{R_{\rm e}} + \frac{1}{R_{\rm m}}. \tag{3}$$

The total Reynolds number is large in the solar atmosphere. We introduce the small parameter ϵ such that $R_{\rm t} = \mathcal{O}(\epsilon^{-2})$. Although at present this scaling seems to be artificial, we shall see in what follows that it is convenient and natural. To explicitly show this scaling in the MHD equations we introduce scaled coefficients of viscosity and magnetic diffusion

$$\nu = \epsilon^{-2}\bar{\nu}, \quad \lambda = \epsilon^{-2}\bar{\lambda}. \tag{4}$$

Then we write the equations of viscous resistive MHD in the form

$$\frac{\partial\rho}{\partial t} + \frac{\partial(\rho u)}{\partial x} = 0, \tag{5}$$

$$\frac{\partial u}{\partial t} + u\frac{\partial u}{\partial x} = -\frac{1}{\rho}\frac{\partial p}{\partial x} - \frac{B_y}{\mu\rho}\frac{\partial B_y}{\partial x} + \epsilon^2\nu\frac{\partial^2 u}{\partial x^2}, \tag{6}$$

$$\frac{\partial v}{\partial t} + u\frac{\partial v}{\partial x} = \frac{B_0}{\mu\rho}\frac{\partial B_y}{\partial x} + \epsilon^2\nu\frac{\partial^2 v}{\partial x^2}, \tag{7}$$

$$\frac{\partial B_y}{\partial t} = \frac{\partial}{\partial x}(vB_0 - uB_y) + \epsilon^2\lambda\frac{\partial^2 B_y}{\partial x^2}, \tag{8}$$

$$\frac{\partial}{\partial t}\left(\frac{p}{\rho^\gamma}\right) + u\frac{\partial}{\partial x}\left(\frac{p}{\rho^\gamma}\right) = 0. \tag{9}$$

Here u and v are the x- and y-components of the velocity, B_y is the y-component of the magnetic field, ρ the density, p the pressure, and γ the adiabatic index. Although the dissipation is present we use the adiabatic equation (9). The reason is that dissipative terms that should appear on the right-hand side of

Eq. (9) are nonlinear and would therefore give higher order corrections to the dynamics of the Alfvén wave. In what follows we only use the linearized form of Eq. (9).

The magnetic cavity is bounded by the two surfaces perpendicular to the background magnetic field at $x = 0$ and $x = L$. The magnetic field is assumed to be frozen in the dense plasmas beyond these boundaries, so that the magnetic field lines follow plasma motions beyond the boundaries. In application to coronal loops, for instance, the boundaries model the dense highly electrically conducting photosphere. We assume that the plasma at $x = L$ is immovable, while it harmonically oscillates in the y-direction at $x = 0$ (Fig. 1). In accordance with this we have the boundary conditions

$$u = v = 0 \quad \text{at} \quad x = L, \tag{10}$$

$$u = 0, \quad v = A\sin(\omega t) \quad \text{at} \quad x = 0, \tag{11}$$

where A and ω are the amplitude and (real) frequency of the driver.

Linear Alfvén waves in the cavity are described by linearized Eqs. (7) and (8). Eliminating B_y from these equations and neglecting terms of the order ϵ^4, we arrive at

$$\frac{\partial^2 v}{\partial t^2} - V_A^2 \frac{\partial^2 v}{\partial x^2} = \epsilon^2(\nu + \lambda)\frac{\partial^3 v}{\partial t \partial x^2}. \tag{12}$$

Let us look for the solution to this equation describing the steady state of driven oscillations. This solution can be looked for in the form $v = \Re(\hat{v}e^{-i\omega t})$, with $\Re$ indicating the real part of a quantity, so Eq. (12) is reduced to

$$\omega^2 \hat{v} + V_A^2 \frac{d^2\hat{v}}{dx^2} = i\epsilon^2\omega(\nu + \lambda)\frac{d^2\hat{v}}{dx^2}. \tag{13}$$

The solution to this equation satisfying boundary conditions (10) and (11) is

$$\hat{v} = \frac{iA\{\exp(ikx) - \exp[ik(2L - x)]\}}{1 - \exp(2ikL)}, \tag{14}$$

where

$$k = \frac{\pi\omega}{L\omega_A[1 - i\epsilon^2\omega V_A^{-2}(\nu + \lambda)]^{1/2}}, \tag{15}$$

with $\omega_A = \pi V_A/L$ the fundamental eigenfrequency of the cavity. The quantity $|\hat{v}(L/2)|$ can be considered as the amplitude of oscillations. To calculate this quantity we use the approximation

$$k \approx \frac{\pi\omega}{L\omega_A}\left[1 + \frac{i\epsilon^2\omega(\nu + \lambda)}{2V_A^2}\right]. \tag{16}$$

Then we obtain from Eq. (14)

$$|\hat{v}\,(L/2)| \approx A|\sin(\pi\omega/2\omega_A)| \times[\sin^2(\pi\omega/\omega_A) + \epsilon^4\omega^4 L^2 V_A^{-6}(\nu + \lambda)^2\cos^2(\pi\omega/\omega_A)]^{-1/2}. \tag{17}$$

As for the case of nonlinear dynamical systems with finite numbers of degree of freedom, the most interesting (i.e. stucturally unstable) behaviour is to be sought in the situation in which nonlinearities, dissipation and driving produce effects which are of the same order (e.g. Guckenheimer and Holmes 1993). This is why, in what follows, we assume that the mistuning is small and oscillations are quasi-resonant: $|\omega/\omega_A - 1| \ll 1$. Then we can write expression (17) in the approximate form

$$|\hat{v}(L/2)| \approx A[\pi^2(\omega/\omega_A - 1)^2 + \epsilon^4\omega^4 L^2 V_A^{-6}(\nu + \lambda)^2]^{-1/2}. \tag{18}$$

When $\omega = \omega_A$ we obtain $|\hat{v}(L/2)| = \mathcal{O}(A\epsilon^{-2})$. On the other hand, when $\nu = \lambda = 0$, that is there is no dissipation, $|\hat{v}(L/2)| = \mathcal{O}(A|\omega/\omega_A - 1|^{-1})$. In what follows we only consider the situation where the two effects, mistuning and dissipation, are of the same order. Therefore we assume that $\omega/\omega_A - 1 = \mathcal{O}(\epsilon^2)$ and write ω in the form

$$\omega = \omega_A(1 + \epsilon^2\Delta). \tag{19}$$

The quantity Δ is called the mistuning parameter.

Linear theory of quasi-resonant oscillations is only valid when the amplitude of oscillations is small. Since this amplitude is of the order $A\epsilon^{-2}$, this condition is equivalent to $A \ll \epsilon^2$. To make analytical progress when studying nonlinear oscillations we assume that the amplitudes of nonlinear oscillations are also small. In what follows we only study the situation where the effect of nonlinearity is of the same order as the effect of dissipation. This implies that the dissipative terms in Eqs. (7) and (8), which are the terms proportional to ν and λ, are of the same order as nonlinear terms. A typical nonlinear term in these equations is $u\partial v/\partial x$. Its ratio to the dissipative term in Eq. (7), which is the term proportional to ν, is of the order $u\epsilon^{-2}$. This ratio is of the order unity when $u = \mathcal{O}(\epsilon^2)$. Let us estimate the order of magnitude of the quantity u in terms of ϵ and A. To do this we analyze how nonlinearity acts. As we have already seen, the amplitude of Alfvén oscillations in the cavity is of the order $A\epsilon^{-2}$. The presence of Alfvén oscillations causes a variation of the total pressure of the order $A^2\epsilon^4$. This variation of the total pressure drives plasma motions which are parallel to the equilibrium magnetic field. The interaction of the longitudinal motion with the basic Alfvén oscillations creates nonlinear corrections to the Alfvén oscillations. Hence, in particular, u is of the order of the total pressure variation, that is $u = \mathcal{O}(A^2\epsilon^{-4})$. Then the condition $u = \mathcal{O}(\epsilon^2)$ leads to $A = \mathcal{O}(\epsilon^3)$. In what follows we take $A = \epsilon^3 V_A$ and rewrite boundary condition (11) as

$$u = 0, \quad v = \epsilon^3 V_A \sin(\omega t) \quad \text{at} \quad x = 0. \tag{20}$$

In the next section we use the set of Eqs. (5)–(9) and boundary conditions (10) and (20) to derive a nonlinear governing equation for quasiresonant Alfvén oscillations in the magnetic cavity.

3. Derivation of the governing equations

To derive the governing equation for nonlinear resonant oscillations in the magnetic cavity we use the singular perturbation method. Since $v = \mathcal{O}(\epsilon^3)$ at the boundary while $v = \mathcal{O}(\epsilon)$ in

the cavity, we can take $v \approx 0$ at $x = 0$ in the main order approximation. In what follows we only consider the steady state of resonant oscillations, where perturbations of all quantities oscillate with the driver's frequency ω. Hence we can expand the quantity v in a Fourier series with respect to x and t:

$$v = \sum_{n=-\infty}^{\infty} e^{in\omega t} \sum_{m=1}^{\infty} v_{nm} \sin \frac{\pi m x}{L}. \tag{21}$$

The fundamental harmonic in this series, represented by terms

$$v_{11} e^{i\omega t} \sin \frac{\pi x}{L} \quad \text{and} \quad v_{-11} e^{-i\omega t} \sin \frac{\pi x}{L},$$

is excited by the driver. All other harmonics in series (21) are generated by the two-step nonlinear mechanism described in Sect. 2. The driving force that appears due to the interaction of the longitudinal motion with the amplitude of the order ϵ^2, and the Alfvén oscillations with the amplitude of the order of ϵ, has amplitude of the order ϵ^3. Then it is straightforward to see that the amplitudes of the higher resonant terms in (21), which are terms with $m = n$, are of the order ϵ, while the non-resonant terms, which are terms with $m \neq n$, are of the order ϵ^3. Hence, we can take v in the form

$$v = \sum_{n=-\infty}^{\infty} v_{nn} e^{in\omega t} \sin \frac{\pi n x}{L} + \mathcal{O}(\epsilon^3). \tag{22}$$

The sum in this equation can be rewritten as

$$\sum_{n=-\infty}^{\infty} v_{nn} e^{in\omega t} \sin \frac{\pi n x}{L} = \epsilon [f(\xi) - f(\eta)], \tag{23}$$

where

$$\xi = \omega t + \frac{\pi x}{L}, \quad \eta = \omega t - \frac{\pi x}{L}, \tag{24}$$

$$f = \sum_{n=-\infty}^{\infty} f_n e^{in\xi}, \quad \epsilon f_n = -\frac{i}{2} v_{nn}. \tag{25}$$

We see that in the main order approximation the nonlinear resonant Alfvén oscillation is represented by a superposition of two nonlinear waves, one of which propagates in the positive direction of the x-axis and the other in the negative direction.

Simple estimates based on Eqs. (5)–(9) show that the perturbations of the quantities ρ and p are of the same order as u, that is of the order ϵ^2, while B_y is of the order ϵ and does not contain terms of the order ϵ^2. Consequently, we look for the solution to the set of Eqs. (5)–(9) in the form of expansions

$$v = \epsilon [f(\xi) - f(\eta)] + \epsilon^3 v^{(3)} + \ldots, \tag{26}$$

$$B_y = \epsilon B_y^{(1)} + \epsilon^3 B_y^{(3)} + \ldots, \tag{27}$$

$$\rho = \rho_0 + \epsilon^2 \rho^{(2)} + \ldots, \tag{28}$$

$$p = p_0 + \epsilon^2 p^{(2)} + \ldots, \tag{29}$$

$$u = \epsilon^2 u^{(2)} + \ldots. \tag{30}$$

Substituting (26)–(30) into Eqs. (5)–(9) we obtain in the first order approximation

$$\begin{aligned} \frac{\partial B_y^{(1)}}{\partial t} &= \frac{\omega B_0}{V_A} \left(\frac{df}{d\xi} + \frac{df}{d\eta} \right), \\ \frac{\partial B_y^{(1)}}{\partial x} &= \frac{\omega B_0}{V_A^2} \left(\frac{df}{d\xi} - \frac{df}{d\eta} \right). \end{aligned} \tag{31}$$

From (31) we get

$$B_y^{(1)} = \frac{B_0}{V_A} [f(\xi) + f(\eta)]. \tag{32}$$

In the second order approximation, with the aid of Eq. (32), we get

$$\frac{\partial \rho^{(2)}}{\partial t} + \rho_0 \frac{\partial u^{(2)}}{\partial x} = 0, \tag{33}$$

$$\frac{\partial u^{(2)}}{\partial t} + \frac{1}{\rho_0} \frac{\partial p^{(2)}}{\partial x} = \frac{\omega}{V_A} [f(\xi) + f(\eta)] \left(\frac{df}{d\xi} - \frac{df}{d\eta} \right), \tag{34}$$

$$p^{(2)} = c_S^2 \rho^{(2)}, \tag{35}$$

where $c_S^2 = \gamma p_0 / \rho_0$ is the square of the sound speed. We eliminate $\rho^{(2)}$ and $p^{(2)}$ from Eqs. (33)–(35) to arrive at

$$\begin{aligned} \frac{\partial^2 u^{(2)}}{\partial t^2} - c_S^2 \frac{\partial^2 u^{(2)}}{\partial x^2} \\ = \frac{\omega}{V_A} \frac{\partial}{\partial t} \left\{ [f(\xi) + f(\eta)] \left(\frac{df}{d\xi} - \frac{df}{d\eta} \right) \right\}. \end{aligned} \tag{36}$$

To solve this equation we use expansion (25) of the function $f(\xi)$ in a Fourier series. In accordance with expression (26) for the velocity, the coefficient f_0 in (25) can be chosen arbitrarily, so that we take $f_0 = 0$. It follows from Eqs. (26) and (32) that

$$f(\xi) = \frac{1}{2} \left(v^{(1)} + \frac{B_0}{V_A} B_y^{(1)} \right), \tag{37}$$

where

$$v^{(1)} = f(\xi) - f(\eta). \tag{38}$$

Since the right-hand side of Eq. (37) is real, the function $f(\xi)$ also has to be real. This leads to the relation

$$f_{-n} = f_n^*. \tag{39}$$

With the aid of (25) we rewrite Eq. (36) as

$$\begin{aligned} \frac{\partial^2 u^{(2)}}{\partial t^2} - c_S^2 \frac{\partial^2 u^{(2)}}{\partial x^2} = \frac{2i\omega^2}{V_A} \sum_{n=-\infty}^{\infty} n e^{in\omega t} \\ \times \sum_{m=-\infty}^{\infty} m f_m f_{n-m} \left[\sin \frac{\pi n x}{L} + \sin \frac{\pi (2m-n) x}{L} \right]. \end{aligned} \tag{40}$$

Since $u^{(2)}$ is a periodic function of t, we can expand $u^{(2)}$ in a Fourier series

$$u^{(2)} = \sum_{n=-\infty}^{\infty} u_n^{(2)}(x) e^{in\omega t}. \tag{41}$$

Then it is straightforward to get from Eq. (40) that $u_0^{(2)} = 0$ and, for $n \neq 0$, the coefficient functions $u_n^{(2)}$ are given by

$$u_n^{(2)} = -2iV_A \left[\frac{1}{n(V_A^2 - c_S^2)} \sum_{m=-\infty}^{\infty} m f_m f_{n-m} \sin\frac{\pi n x}{L} + n \sum_{m=-\infty}^{\infty} \frac{m f_m f_{n-m}}{V_A^2 n^2 - c_S^2 (2m-n)^2} \sin\frac{\pi(2m-n)x}{L} \right]. \quad (42)$$

The quantity $u_n^{(2)}$ is singular if V_A/c_S is a rational number. From the physical point of view this singularity is related to the resonance between a harmonic of the standing Alfvén wave and a harmonic of the standing sound wave. In general dissipation removes the singularity. However in our approach dissipation does not do this because, in accordance with the basic assumption, it appears in the third order approximation only. When the plasma is only weakly dissipative $u_n^{(2)}$ takes finite but large value if the resonant condition is satisfied for some terms on the right-hand side of Eq. (42). In Sect. 2 it was explained that the isotropic shear viscosity can be used when studying Alfvén oscillations. However this is not true for sound waves. For typical conditions in the upper part of the chromosphere and especially in the corona damping of sound waves is mainly caused by the viscosity described by the first term of the Braginskii's tensorial expression (Braginskii 1965) and by the thermal conductivity along the magnetic field lines. These two dissipative processes are strong enough, so that for sound waves the solar coronal plasma is not weakly dissipative at all. This difference in the dissipative mechanisms for Alfvén waves and sound waves results, e.g., in that coronal loops are high quality resonators for Alfvén waves, while they are only low quality resonantors for sound waves. Hence the account of viscosity and thermal conductivity completely removes possible resonances between Alfvén and sound waves. To avoid complications related to the consideration of sound wave damping we assume in our analysis that V_A/c_S is an irrational number. Then expression (42) does not contain singular terms.

In what follows we also use the quantity $\rho^{(2)}$. With the aid of Eqs. (41) and (42) we obtain from Eq. (33)

$$\rho^{(2)} = \sum_{n=-\infty}^{\infty} \rho_n^{(2)}(x) e^{in\omega t}, \quad (43)$$

where the coefficient functions $\rho_n^{(2)}(x)$ with $n \neq 0$ are given by

$$\rho_n^{(2)} = -\frac{2\rho_0}{n(V_A^2 - c_S^2)} \sum_{m=-\infty}^{\infty} m f_m f_{n-m} \cos\frac{\pi n x}{L} + 2\rho_0 \sum_{m=-\infty}^{\infty} \frac{m(2m-n) f_m f_{n-m}}{V_A^2 n^2 - c_S^2 (2m-n)^2} \cos\frac{\pi(2m-n)x}{L}. \quad (44)$$

Eq. (33) does not determine the coefficient function $\rho_0^{(2)}$. To determine this function we use Eqs. (34) and (35). In addition we assume that the mean value of $\rho_0^{(2)}$ over the interval $[0, L]$ is zero because otherwise we can include this mean value in the unperturbed density ρ_0. Then we obtain

$$\rho_0^{(2)} = -\frac{\rho_0}{c_S^2} \sum_{m=-\infty}^{\infty} |f_m|^2 \cos\frac{2\pi m x}{L}. \quad (45)$$

In the third order approximation we collect terms of the order ϵ^3 in Eqs. (7) and (8). As a result we get

$$\frac{\partial v^{(3)}}{\partial t} - \frac{\omega^2 L^2}{\pi^2 B_0} \frac{\partial B_y^{(3)}}{\partial x} = -\frac{2V_A^2 \Delta}{B_0} \frac{\partial B_y^{(1)}}{\partial x} - u^{(2)} \frac{\partial v^{(1)}}{\partial x} - \frac{V_A^2}{\rho_0 B_0} \rho^{(2)} \frac{\partial B_y^{(1)}}{\partial x} + \nu \frac{\partial^2 v^{(1)}}{\partial x^2}, \quad (46)$$

$$\frac{\partial B_y^{(3)}}{\partial t} - B_0 \frac{\partial v^{(3)}}{\partial x} = -\frac{\partial}{\partial x}(u^{(2)} B_y^{(1)}) + \lambda \frac{\partial^2 B_y^{(1)}}{\partial x^2}. \quad (47)$$

Eliminating $B_y^{(3)}$ from these equations and using Eqs. (31) we obtain

$$\frac{\partial^2 v^{(3)}}{\partial t^2} - \frac{\omega^2 L^2}{\pi^2 B_0} \frac{\partial^2 v^{(3)}}{\partial x^2} = F, \quad (48)$$

where

$$F = -2\Delta \frac{\partial^2 v^{(1)}}{\partial t^2} - \frac{\partial}{\partial t}\left(u^{(2)} \frac{\partial v^{(1)}}{\partial x} - \frac{\rho^{(2)}}{\rho_0} \frac{\partial v^{(1)}}{\partial t} \right) - \frac{V_A^2}{B_0} \frac{\partial^2}{\partial x^2}\left(u^{(2)} B_y^{(1)} \right) + (\nu + \lambda) \frac{\partial^3 v^{(1)}}{\partial t \partial x^2}. \quad (49)$$

The function $v^{(3)}$ satisfies the boundary conditions

$$v^{(3)} = 0 \quad \text{at} \quad x = L, \quad (50)$$

$$v^{(3)} = V_A \sin(\omega t) \quad \text{at} \quad x = 0. \quad (51)$$

In order to have homogeneous boundary conditions we make substitution

$$v^{(3)} = g + V_A \left(1 - \frac{x}{L}\right) \sin(\omega t). \quad (52)$$

Then we rewrite Eq. (48) as

$$\frac{\partial^2 g}{\partial t^2} - \frac{\omega^2 L^2}{\pi^2 B_0} \frac{\partial^2 g}{\partial x^2} = F + V_A \omega^2 \left(1 - \frac{x}{L}\right) \sin(\omega t). \quad (53)$$

The function g satisfies the boundary conditions

$$g = 0 \quad \text{at} \quad x = 0 \quad \text{and} \quad x = L. \quad (54)$$

Now we expand the functions g and F in Fourier series with respect to time:

$$g = \sum_{n=-\infty}^{\infty} g_n e^{in\omega t}, \quad F = \sum_{n=-\infty}^{\infty} F_n e^{in\omega t}. \quad (55)$$

The substitution of these expansions into (53) yields

$$\frac{\partial^2 g_n}{\partial x^2} + \frac{\pi^2 n^2}{L^2} g_n = -\frac{F_n}{V_A^2} + \frac{i\omega^2}{2V_A} \left(1 - \frac{x}{L}\right) (\delta_{1,n} - \delta_{-1,n}), \quad (56)$$

where $\delta_{j,n}$ is the Kronecker delta-symbol. Eq. (56) is compatible only when its right-hand side is orthogonal to the eigenfunction of the differential operator that is determined by the left-hand side of Eq. (56) and boundary conditions (54). This eigenfunction is $\sin(\pi n x/L)$, so that the orthogonality condition takes the form

$$\int_0^L F_n \sin\frac{\pi n x}{L}\,dx = \frac{i\omega^2 L V_A}{2\pi}(\delta_{1,n}+\delta_{-1,n}). \quad (57)$$

With the use of Eqs. (32), (38), (39), (42), (44), (45), and (49) we rewrite this equation for $n>0$ as

$$2\Delta f_n - \frac{i\omega(\nu+\lambda)}{V_A^2} n f_n - \frac{(f^3)_n}{2(V_A^2-c_S^2)} - f_n \sum_{m=-\infty}^{\infty} \frac{(2n-m)^2|f_{n-m}|^2}{V_A^2 m^2 - c_S^2(2n-m)^2} = \frac{V_A\delta_{1,n}}{2\pi}, \quad (58)$$

where $(f^3)_n$ is the nth Fourier coefficient for the function f^3. For $n<0$ the Fourier coefficients are determined by the relation $f_n = f^*_{-n}$.

Eq. (58) is the nonlinear governing equation for the function f written in terms of the Fourier coefficients of this function. In Sect. 5 we analytically study this equation in the one-mode approximation; in Sect. 6 we present results of its numerical solution in the multi-mode case. Here we only note one very important property of Eq. (58). If we take the approximation of cold plasmas and put $c_S = 0$, we obtain that the sum in (58) becomes singular since its term corresponding to $m=0$ is infinite. This property implies that in a cold plasma the steady state of driven oscillations cannot be attained.

4. Energetics

In this section we calculate the energy dissipated and the energy stored in the magnetic cavity. Since the cavity has an infinite extension in the y- and z-direction, we calculate the energy averaged over one period dissipated in a volume with the length L in the x-direction and with the unit lengths in the y- and z-direction. In the steady state of driven oscillations this energy is equal to the energy flux through the unit area of the surface $x=0$ averaged over one period. Since the x-component of the velocity is zero at $x=0$, the instantaneous energy flux through the unit area of the surface $x=0$ is given by the Poynting vector $\boldsymbol{E}\times\boldsymbol{B}/\mu$, where $\boldsymbol{E}$ is the electric field. With the use of the Ohm's and Ampere's laws we get

$$\boldsymbol{E}\times\boldsymbol{B} = \boldsymbol{v}B^2 - \boldsymbol{B}(\boldsymbol{v}\cdot\boldsymbol{B}) + \epsilon^2\lambda(\nabla\times\boldsymbol{B})\times\boldsymbol{B}. \quad (59)$$

With the aid of Eqs. (20) and (27) we find that at $x=0$

$$(\boldsymbol{E}\times\boldsymbol{B})_x = -\epsilon^4 V_A B_0 B_y^{(1)}\sin(\omega t) - \epsilon^4\lambda B_y^{(1)}\frac{\partial B_y^{(1)}}{\partial x} + \mathcal{O}(\epsilon^6). \quad (60)$$

Now we use Eq. (32) to reduce this expression to

$$(\boldsymbol{E}\times\boldsymbol{B})_x = -2\epsilon^4 B_0^2 f(\omega t)\sin(\omega t) + \mathcal{O}(\epsilon^6). \quad (61)$$

And, finally, we arrive at the following expression for the period-averaged energy flux $\mathcal{S}$:

$$\mathcal{S} = \frac{\omega}{2\pi\mu}\int_0^{2\pi/\omega}(\boldsymbol{E}\times\boldsymbol{B})_x\,dt = -\frac{\epsilon^4 V_A^2\rho_0}{\pi}\int_0^{2\pi} f(\tau)\sin(\tau)\,d\tau + \mathcal{O}(\epsilon^6). \quad (62)$$

This expression can be also rewritten in the alternative form

$$\mathcal{S} = 2\epsilon^4\rho_0 V_A^2\Im(f_1) + \mathcal{O}(\epsilon^6), \quad (63)$$

where the symbol $\Im$ indicates the imaginary part of a quantity.

When $n<0$ the equation for f_n is obtained from Eq. (58) by substituting $\delta_{-1,n}$ for $\delta_{1,n}$. We multiply the equation for f_n by nf_n^* and make the summation with respect to n. As a result we obtain

$$\frac{V_A}{2\pi}(f_1^*-f_1) = 2\Delta\sum_{n=-\infty}^{\infty} n|f_n|^2 - \frac{i\omega(\nu+\lambda)}{V_A^2}\sum_{n=-\infty}^{\infty} n^2|f_n|^2 - \frac{1}{2(V_A^2-c_S^2)}\sum_{n=-\infty}^{\infty} n f_n^*(f^3)_n - \sum_{n=-\infty}^{\infty} n|f_n|^2\sum_{m=-\infty}^{\infty}\frac{(2n-m)^2|f_{n-m}|^2}{V_A^2m^2-c_S^2(2n-m)^2}, \quad (64)$$

where $(f^3)_n$ is the Fourier coefficient of the function f^3. It is straightforward to show that the first and the last term on the right-hand side of this equation are zero. With the use of the Parseval identity we obtain

$$-2\pi i\sum_{n=-\infty}^{\infty} n f_n^*(f^3)_n = \int_0^{2\pi} f^3\frac{\partial f}{\partial\xi}\,d\xi = 0. \quad (65)$$

Then it follows from Eq. (64) that

$$\Im(v_1) = \frac{\pi\omega(\nu+\lambda)}{V_A^3}\sum_{n=-\infty}^{\infty} n^2|f_n|^2 > 0, \quad (66)$$

so the energy flux $\mathcal{S}$ into the cavity is positive as can be expected from a physical point of view. The period-averaged energy stored in the volume of the magnetic cavity with the length L in the x-direction and with the unit lengths in the y- and z-direction is

$$\mathcal{E} = \frac{\epsilon^2\omega}{4\pi}\int_0^{2\pi/\omega} dt\int_0^L\left[\rho_0(v^{(1)})^2 + \frac{1}{\mu}(B_y^{(1)})^2\right]dx + \mathcal{O}(\epsilon^4). \quad (67)$$

When deriving this equation we have used the fact that the contribution of the perturbation of the inner energy of the plasma into the stored energy is of the order $\mathcal{O}(\epsilon^4)$. We use Eqs. (32), (38), and (39) to transform expression (67) to

$$\mathcal{E} = 4\epsilon^2\rho_0 L\sum_{n=1}^{\infty}|f_n|^2 + \mathcal{O}(\epsilon^4). \quad (68)$$

It is interesting to note that $\mathcal{S}/\mathcal{E} = \mathcal{O}(\epsilon^2)$.

When $\epsilon^2 R_{\rm t} \ll 1$ (however $R_{\rm t} \gg 1$), so that the nonlinear terms in Eq. (58) can be neglected in comparison with the linear dissipative term, it follows from Eq. (58) that $f_n = 0$ for $|n| > 1$. Then the expressions for $\mathcal{S}$ and $\mathcal{E}$ take the forms

$$\mathcal{S} = \frac{\epsilon^4 \rho_0 V_A^6 (\nu + \lambda)}{L[4\Delta^2 V_A^4 + \omega^2 (\nu + \lambda)^2]}, \tag{69}$$

$$\mathcal{E} = \frac{\epsilon^2 \rho_0 V_A^6 L}{\pi^2 [4\Delta^2 V_A^4 + \omega^2 (\nu + \lambda)^2]}. \tag{70}$$

In the next sections expressions (63) and (68) are used to calculate the energy flux into the cavity and the energy stored in the cavity analytically in the one-mode approximation and numerically in the multi-modal case.

5. Multistability

The nonlinear algebraic system (58) has in general multiple solutions. This fact holds true even in the 1–mode approximation. Let us introduce the dimensionless quantities

$$V = \frac{f}{V_A}, \quad \beta = \frac{c_S^2}{V_A^2}, \quad R = \frac{V_A^2}{\omega(\nu + \lambda)}. \tag{71}$$

In accordance with the assumption made in Sect. 3 the quantity $\beta^{1/2}$ is an irrational number. The quantity $R = \epsilon^2 R_{\rm t}/\pi$ can be called the scaled total Reynolds number.

5.1. One-mode approximation

Let us consider the one-mode approximation where $v_n = 0$ for $|n| > 1$. Then it is straightforward to obtain

$$(V^3)_1 = 3V_1 |V_1|^2, \quad \sum_{m=-\infty}^{\infty} \frac{(2-m)^2 |V_{1-m}|^2}{m^2 - \beta(2-m)^2} = -\frac{|V_1|^2}{\beta}. \tag{72}$$

With the use of these results we get from Eq. (58)

$$V_1 \left(2\Delta + \frac{2 - 5\beta}{2\beta(1-\beta)} |V_1|^2 - iR^{-1} \right) = \frac{1}{2\pi}. \tag{73}$$

The quantity V_{-1} is determined by the relation $V_{-1} = V_1^*$. We multiply Eq. (73) by the complex conjugate equation to derive the equation for $|V_1|^2$

$$Y^3 + 2Y^2 + (1 + 3\kappa)Y - C = 0, \tag{74}$$

where we have introduced the notation

$$Y = \frac{2 - 5\beta}{4\Delta\beta(1-\beta)} |V_1|^2, \quad \kappa = \frac{1}{12\Delta^2 R^2}, \tag{75}$$

$$C = \frac{2 - 5\beta}{64\pi^2 \Delta^3 \beta(1-\beta)}. \tag{76}$$

In what follows we assume that $\beta < 2/5$. We also assume that $\Delta \neq 0$. The case where $\Delta = 0$ will be considered separately.

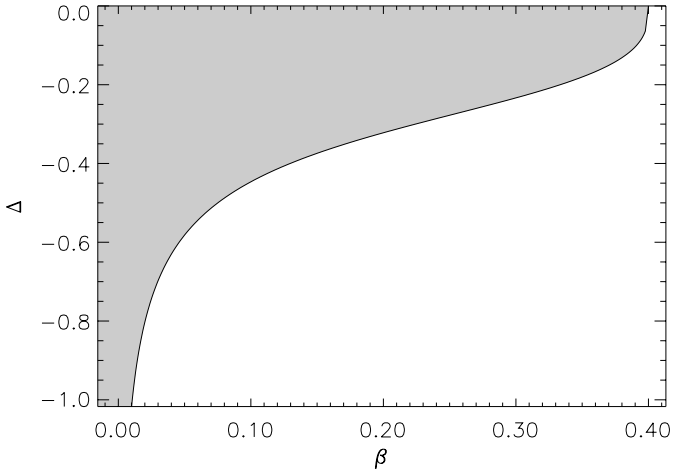

Fig. 2. The dependence of Δ_c on β. Unique solutions exist in the shaded area. In the non-shaded area either unique or triple solutions exist depending on the value of R.

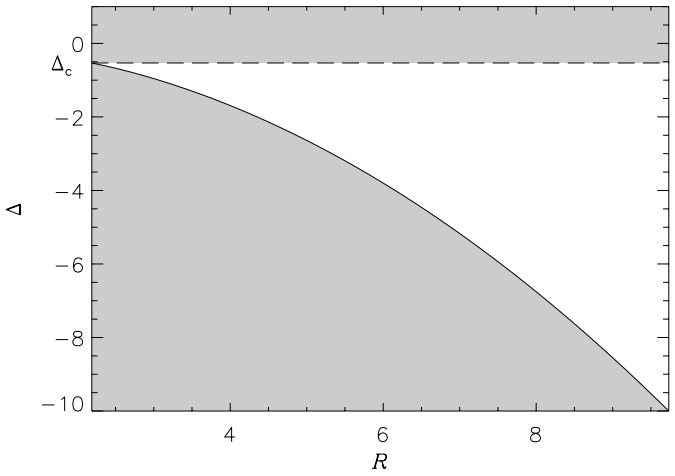

Fig. 3. The dependence of Δ_R on R for $\beta = 0.1$ (solid line). Unique (triple) solutions exist in the shaded (non-shaded) area.

Since $|V_1|^2 > 0$ we are looking for solutions to Eq. (74) satisfying the condition $Y \mathrm{sign}\Delta > 0$. When $\Delta > 0$ the polynomial on the left-hand side of Eq. (74) is a monotonically growing function for $Y > 0$. Since $C < 0$ there is exactly one positive root to Eq. (74).

When $\Delta < 0$ the analysis is more complicated. Now we look for negative roots to Eq. (74) and it is straightforward to see that all real roots to this equation are negative. The discriminant of this equation is

$$D = \sigma^3 + \sigma^2 + 2d\sigma + d^2, \tag{77}$$

where

$$\sigma = \kappa - \frac{1}{9}, \quad d = \frac{1}{2}C + \frac{4}{27}. \tag{78}$$

Eq. (74) has one real root when $D > 0$ and three real roots when $D < 0$. The discriminant of the cubic equation $D(\sigma) = 0$ is $\frac{1}{4}d^3(d - \frac{4}{27})$. Since $C < 0$ the quantity d satisfies the restriction $d < \frac{4}{27}$. We consider two cases:

i) $d < 0$. In this case there is only one real root σ_1 to the equation $D(\sigma) = 0$. $D(\sigma) < 0$ when $\sigma < \sigma_1$, while $D(\sigma) > 0$ when $\sigma > \sigma_1$. Since $D(-\frac{1}{9}) > 0$, the root σ_1 satisfies the inequality $\sigma_1 < -\frac{1}{9}$. The condition $\kappa > 0$ leads to $\sigma > -\frac{1}{9} > \sigma_1$. Hence, for all possible values of σ we have $D(\sigma) > 0$. This implies that there is only one real root to Eq. (74).

ii) $0 < d < \frac{4}{27}$. Then there are three real roots $\sigma_1 < \sigma_2 < \sigma_3 < 0$ to Eq. (77). It is obvious that $D < 0$ when either $\sigma < \sigma_1$ or $\sigma_2 < \sigma < \sigma_3$, while $D > 0$ otherwise. Since $\sigma_1 + \sigma_2 + \sigma_3 = -1$, it follows that $\sigma_1 < -\frac{1}{3}$. Since $D(-\frac{1}{9}) < 0$ we obtain that $\sigma_2 < -\frac{1}{9} < \sigma_3$. Since $\sigma > -\frac{1}{9}$ it follows that $D < 0$ when $\sigma < \sigma_3$, while $D > 0$ when $\sigma > \sigma_3$. Hence, Eq. (74) has one real root when $\sigma < \sigma_3$ and three real roots when $\sigma > \sigma_3$.

Summarizing the analysis we state that there are three real roots to Eq. (74) when the following two inequalities are satisfied:

$$-\frac{8}{27} < C < 0, \quad 0 < \kappa < \sigma_3 + \frac{1}{9}. \tag{79}$$

If at least one of them is not satisfied, there is only one real root to Eq. (74). Examples of unique and triple solutions are shown in Figs. 4*a* and 4*b* respectively.

In terms of Δ and R inequalities (79) are rewritten as

$$\Delta_R(\beta, R) < \Delta < \Delta_c(\beta) \equiv -\frac{3}{8}\left[\frac{2-5\beta}{\pi^2\beta(1-\beta)}\right]^{1/3}, \tag{80}$$

where $\Delta_R(\beta, R)$ is obtained inverting the relation

$$R = \frac{1}{2|\Delta_R|}\left(\frac{3}{1+9\sigma_3(\Delta_R)}\right)^{1/2}. \tag{81}$$

Note that the dependence Δ_R on R is given by the asymptotic formula

$$\Delta_R \simeq -\frac{R^2}{8\pi^2}\frac{2-5\beta}{\beta(1-\beta)}, \text{ for } 1 \ll R < \epsilon^{-1/2} \tag{82}$$

The upper bound on R is needed since the quasiresonant perturbation scheme adopted in Eq. (19) requires $\max|\Delta| = \mathcal{O}(\epsilon^{-1})$.

It can be seen that the equation for $|V_1|^2$ has only one positive real root for all values of R when $\Delta = 0$. The dependencies of Δ_c on β and Δ_R on R for $\beta = 0.1$ are shown in Figs. 2 and 3 respectively.

We use Eq. (73) to rewrite expressions (63) and (68) for the Poynting flux and the energy in the cavity as

$$\mathcal{S} = \epsilon^4\rho_0 V_A^3 S, \quad \mathcal{E} = \epsilon^2\rho_0 L V_A^2 E, \tag{83}$$

where

$$S = \frac{(3\kappa)^{1/2}}{\pi|\Delta|[(1+Y)^2+3\kappa]}, \quad E = \frac{1}{\pi^2\Delta^2[(1+Y)^2+3\kappa]}. \tag{84}$$

In Figs. 4b and 5b the dependencies of the quantities S and E on R are shown for $\beta = 0.1$ and $\Delta = 0.3$ and $\Delta = -1$ respectively. It is seen from formulæ (84) (75) that $S \propto 1/R$ and $E \to \text{const}$ as $R \to \infty$. This trend is in good agreement with Figs. 4b and 5b.

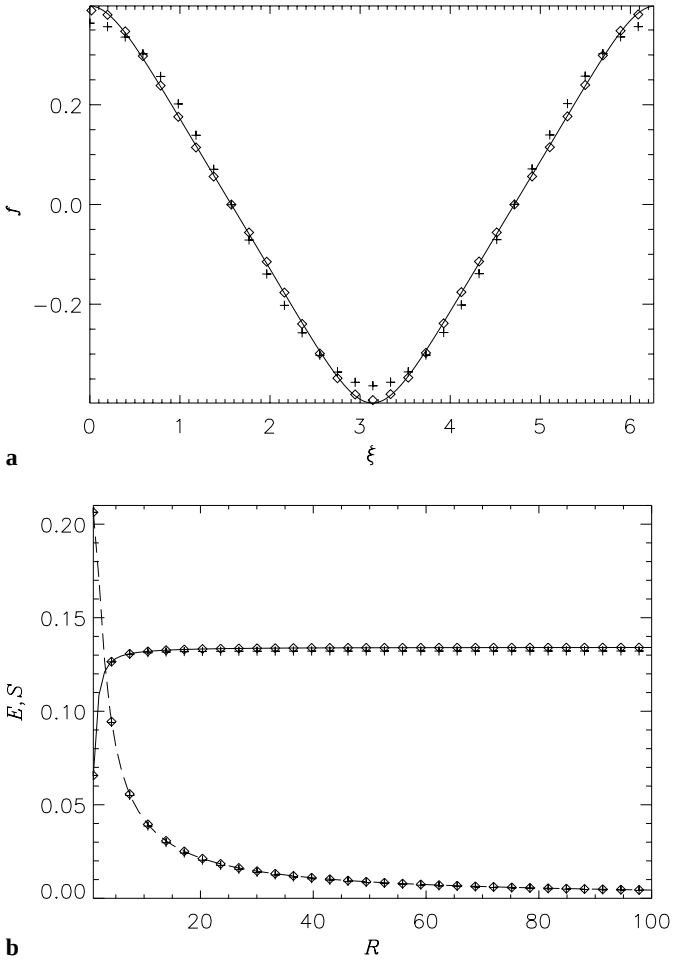

Fig. 4a and b. A unique stationary state for $\beta = 0.1$ and $\Delta = 0.3$. **a** f vs ξ for $R = 1000$. The solid line shows the numerical solution obtained with the use of 128 modes. **b** The dimensionless energy, E, (solid line) and Poynting flux, S, (dashed line) vs the normalized Reynolds number R calculated numerically with the use of 128 modes. In both figures $+$ and $\diamond$ shows the 1-mode (analytical) and the 4-mode (numerical) solutions respectively.

One peculiarity of systems with multiple solutions is their ability to 'bifurcate' from one equilibrium state to another, one classical example being the nonlinear Duffing oscillator. This indeed happens in our hydromagnetic cavity, as it can be seen in Figs. 5b and 6. The transitions the system experiences in going from one 'branch' of the response curve to the other imply an energy dissipation if the arrival branch has a lower energy than the starting branch. When $R \gg 1$ the transition takes place for $|\Delta| = |\Delta_R| \gg 1$, so that, from Eqs. (74), (82) and (84)

$$E = \frac{4R^2}{\pi^2} + \mathcal{O}(R), \quad \text{upper branch},$$
$$E = \mathcal{O}(R^{-4}), \quad \text{lower branch}, \tag{85}$$

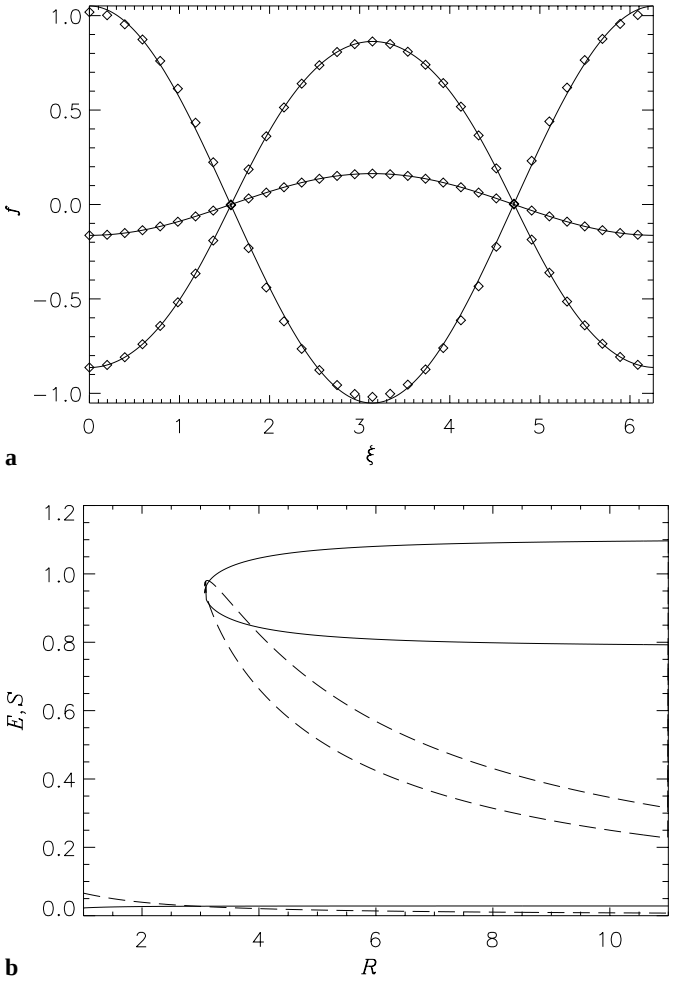

Fig. 5. **a** f computed using Eq. (25) with 128 modes for $\beta = 0.1$, $\Delta = -1$, and $R = 1000$. The three curves correspond to the three different solutions to Eq. (58). $\diamond$ shows the 1-mode (analytical) solution. **b** Bifurcation diagrams for Eq. (58). The dimensionless energy, E, (solid line) and Poynting flux, S, (dashed line) vs the normalized Reynolds number R for $\beta = 0.1$ and $\Delta = -1$. Note the coalescence of the upper two branches at $R \approx 3$.

and the energy jump is

$$\Delta E = \frac{4R^2}{\pi^2} + \mathcal{O}(R). \tag{86}$$

The time in which this energy is dissipated depends on the details of the dynamics in the neighbourhood of the stationary states: its estimate is $\mathcal{O}((R/\epsilon^2)L/V_A)$. Taking Eq. (86) into account we may write the following estimate for the released power:

$$\mathcal{W} \approx \epsilon^4 \rho_0 V_A^3 W, \quad W = \frac{4}{\pi^2} R. \tag{87}$$

The quantity W is comparable with the normalized Poynting flux (84) at the bifurcation point of the upper branch ($\Delta = \Delta_R$), i.e.

$$S = \frac{2}{\pi} R. \tag{88}$$

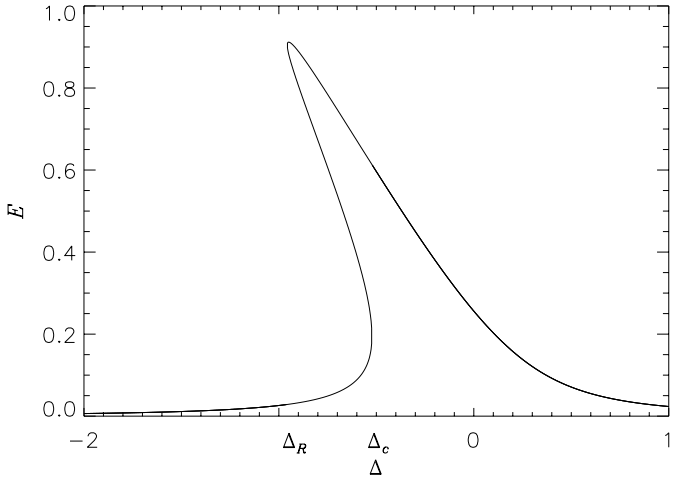

Fig. 6. Energy response of the cavity vs the normalized frequency mistuning at $\beta = 0.1$ and $R = 3$. Note the similarity with the response curve of the Duffing oscillator.

We recall that in (87) and (88) $R < \epsilon^{-1/2}$, in accordance with the consistency constraint of Eq. (82).

5.2. Numerical results

To solve the infinite set of algebraic Eqs. (58) we have used the following method. First we truncated this set of equations and take $f_n = 0$ for $|n| > N$. The relation $f_n = f^*_{-n}$ and the fact that $f_0 = 0$ enabled us to consider $n > 0$ only. As a result we have to solve a set of N algebraic equations. We use the Newton–Raphson method to solve this set of equations (Press et al. 1992). Convergence of this method is highly improved if a 'good' initial guess is given for the root. It turned out that for values of Δ out of the narrow window $[0.20,\ 0.23]$ the low-modal approximation gives a very good initial guess. In Figs. 4 and 5 numerical results for $R = 1000$ and $\Delta = 0.3$ and $\Delta = -1$ are shown. These results were obtained with $N = 128$. We see that the one-mode solution gives an excellent approximation for the multi-modal solution. We have scanned a wide range of R and $\Delta \notin [0.20,\ 0.23]$ and obtained the same result: the low-modal and multi-modal solutions practically coincide. Hence, we conclude that the low-mode approximation provides a very good description of the steady state of Alfvén oscillations in the magnetic cavity unless $0.20 \leq \Delta \leq 0.23$.

6. Solutions with shocks

When $0.20 \leq \Delta \leq 0.23$ the one-mode approximation does not give a good initial guess for large values of R. To find this initial guess we have used the following procedure. First we found a solution for a small value of R, where the one-mode analytical solution is an acceptable initial guess. Then we increased R and used the solution for the previous value of R as a guess. This procedure was iterated until R reached the desired value. The function $f(\xi)$ for $\beta = 0.1$, $\Delta = 0.2$, and $R = 10,\ 100,\ \text{and}\ 1000$ is shown in Fig. 7a. We see that the

solution for $R = 1000$ is characterized by very large spatial gradients. As a matter of fact regions with these large spatial gradients correspond to shock waves for $R \to \infty$.

Once the solution f_n is found, we can reconstruct the velocity field $v(x,t)$ using Eq. (22). The time evolution of the velocity $v(x,t)$ is shown in Fig. 7b.

The progressive build-up of larger and larger gradients as R increases is not the only way in which shocks may arise. In Fig. 8a the function $f(\xi)$ is shown for $\beta = 0.1$, $\Delta = 0.22$, and $R = 160$ and $R = 160.5$. Note the transition from the smooth solution at $R \simeq 160.5$ to the solution containing large gradients (shocks) at $R \simeq 160$. The former is a low-modal solution. To show this, we took its Fourier transform in ξ and we truncated it up to mode 3 included; then we inverted the truncated transform. The results are labelled by $\diamond$ in Fig. 8a.

To better understand the transition from the low-modal solution to the shock solution, we solved Eq. (58) for $\Delta = 0.22$ and R varying from 10 to 500. In Fig. 8b the dependences of E and S on R are shown. We see that while these is a unique solution for $R < R_c \approx 160$, there exists a second solution for $R > R_c$, so that a bifurcation takes place at $R = R_c$. The transition from the smooth solution at $R = 160.5$ to the shock solution at $R = 160$ corresponds to the jump from the lower solid curve to the upper one in the energy diagram. (Fig. 8b, upper panel).

In accordance with the general theory of bifurcations, a single new solution cannot be born as a result of a saddle-node bifurcation. New solutions are born in pairs. This implies that there must be the third solution when $R > R_c$. This hypothetical third solution is shown in Fig. 8b by the short-dashed lines. Unfortunately, analytical theory does not provide a good guess for this hypothetical solution. The iterative procedure used to obtain the shock solutions is also inapplicable. As a result, to the best of our abilities, we were unable to compute the hypothetical third solution numerically.

In shock solutions the energy buildup and dissipation in the cavity deviate from the asymptotic behaviour described in the previous section. Rather it is seen that both E and S increase linearly with R for $30 < R < 200$. Then, when R is increased further, the Poynting flux is saturated. It is a typical behaviour in the presence of shock waves. When dissipative coefficients are decreased, the shock structure becomes thinner. This leads to the enhancement of spatial gradients in the shock structure. As a result the amount of energy dissipated in the shock wave remains constant.

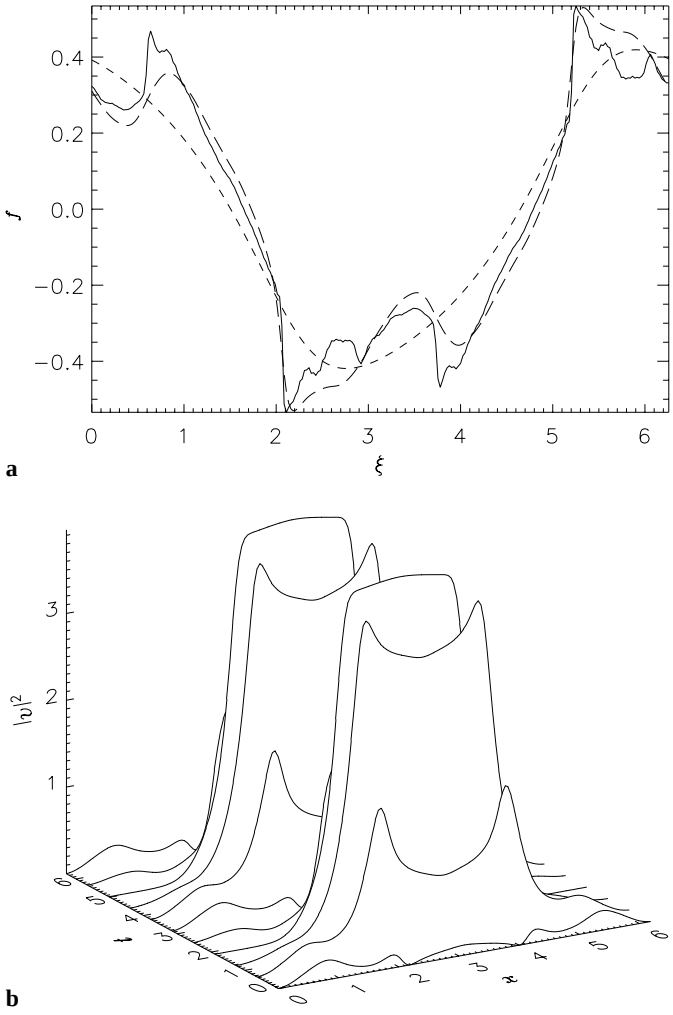

Fig. 7a and b. The solutions with shocks for $\beta = 0.1$ and $\Delta = 0.2$. **a**. f vs ξ numerically calculated with $N = 128$. Note the progressive development of shocks as R is increased from 10 (short-dashed line) to 100 (long-dashed line) and 1000 (solid line). **b.** The time-evolution of the velocity field $v(x,t)$ for $R = 100$.

7. Conclusions

In the present paper we addressed the problem of nonlinear propagation of MHD waves in regions of the solar atmosphere where the plasma can be considered as forming a hydromagnetic cavity embedded in a magnetic field. We studied the stationary response of the cavity to the excitation of Alfvén waves in its interior by the oscillatory motion of one of its boundaries.

The main result of our work are:

- Stationary states exist which can be modelled, to a remarkable accuracy, by the superposition of very few (even one) spatial Fourier components. This fact substantiates the earlier efforts, relying on mode–truncated Fourier analysis (Nocera & Priest 1991; Nocera 1994; Nocera et al. 1997; Bologna & Nocera 1998).
- Hydromagnetic shocks are also admitted as solutions. This fact seems to carry the results by Carlsson & Stein (1997) – obtained in the framework of radiative hydrodynamics – into the hydromagnetic regime.
- Shocks exist in a narrow range of parameters and this could explain why their manifestation as chromospheric bright points is rarer than numerical simulations would suggest.
- Bifurcations (catastrophes) between the low–modal solutions and between these and the shock solutions exist as parameters are varied. This can be invoked as a mechanism to trigger abrupt phenomena in the solar atmosphere.

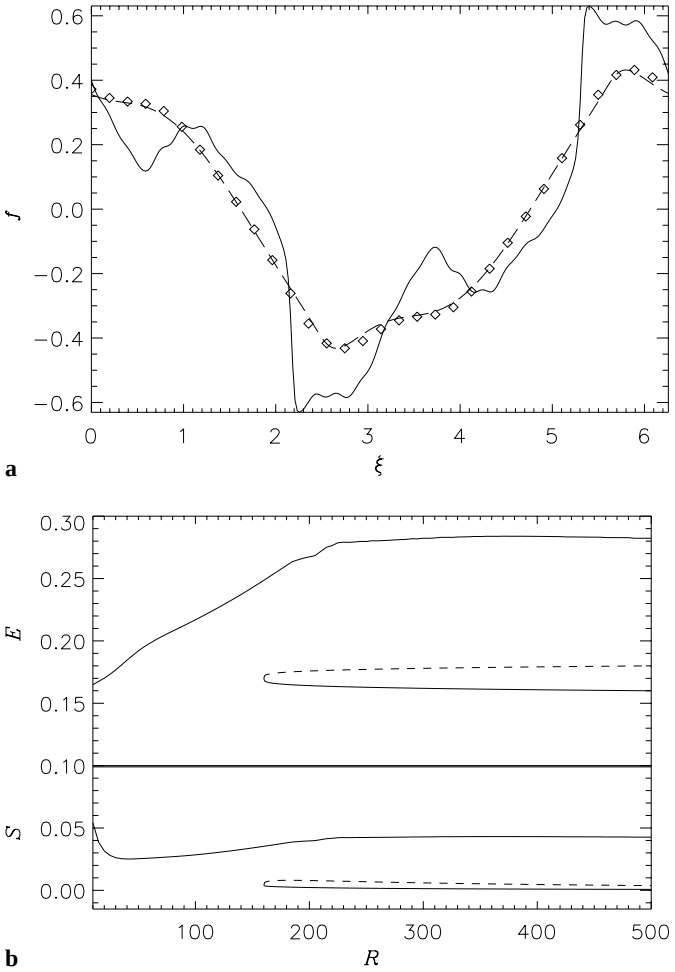

Fig. 8a and b. The transition from the low–modal solution to the shock solution for $\beta = 0.1$ and $\Delta = 0.22$. Solutions were obtained with the use of $N = 128$. **a**. f vs ξ. The solid line corresponds to $R = 160$ and the dashed line to $R = 160.5$. The $\diamond$ corresponds to the 3-mode approximation at $R = 160.5$. **b** upper panel. The dimensionless energy, E, vs the normalized Reynolds number R. **b** lower panel. The Poynting flux, S. The upper solid curve in both panels of **b** corresponds to shock solutions and the lower solid curve to low–modal solutions. The dashed curve corresponds to the hypothetical third low–modal solution (see text). Note the saturation of E for both types of solutions. S is saturated for the shock solutions. Although it is not clearly seen in the figure, we checked that $S \propto 1/R$ for the low-modal solutions.

– Turbulent stationary states (namely states with a power-law spatial spectrum) are not found in our investigation. We conclude that, if they exist, they must have a dynamic nature.

Two key parameters govern the behaviour of the cavity, namely the re-scaled Reynolds number R and the re-scaled mistuning Δ between the frequency of the boundary oscillations and the frequency of the fundamental Alfvén mode of the cavity. The values of the actual Reynolds number and mistuning are obtained by dividing R and multiplying Δ by ϵ^2, where ϵ^3 is the Alfvén Mach number of the velocity amplitude at the cavity's moving boundary. The third parameter of our problem (the plasma β) plays a less critical role, so that we have taken $\beta = 0.1$.

The response of the cavity as a function of R and Δ appears to be multivalued and a first exploration reveals that:

– The low-modal states set in for all values of Δ. For $\Delta_R(\beta, R) < \Delta < \Delta_c(\beta) < 0$ it was shown analytically that they occur in triplets (two stable and one unstable) and give rise to multistability (like in the Duffing oscillator).
– For $\Delta_c < \Delta < \Delta_{s1} \simeq 0.2$ and for all values of R they are unique.
– For $\Delta_{s1} < \Delta < \Delta_{s2} \simeq 0.23$ they exist alongside with solutions which exhibit large gradients (shocks). The build-up of large gradients may develop starting from smooth states in either an 'ordinary' continuous way, as R is increased, or in a 'catastrophic' way: in this latter scenario, a low-modal solution becomes unstable as R is decreased below a critical value where it bifurcates to a stable shock solution. For $\Delta = 0.22$ we have computed this value to lie in the range $160 < R < 160.5$.
– For $\Delta > \Delta_{s2}$, once again, only the unique low-modal solutions exist.
– For a fixed Δ the energy content of the cavity, $\mathcal{E}$, is saturated as R is increased. For the low-modal oscillatory state it was shown analytically that the saturated energy value is proportional to ϵ^2.
– For the low-modal solutions, the Poynting flux $\mathcal{S}$ is proportional to $1/R$, i.e. to the sum of coefficients of viscosity and magnetic diffusion. On the other hand, for the shock solutions, which appear in the range $\Delta_{s1} < \Delta < \Delta_{s2}$, $\mathcal{S}$ is saturated when R is increased.
– Thus, for $\Delta_{s1} < \Delta < \Delta_{s2}$, when both the low-modal and the shock solutions exist, the energy dissipation rate is highest in the shock structures, provided R is large enough.

This latter result is in agreement with the idea of chromospheric bright points being driven by shocks. However, at variance with the traditional scenario of radiative hydrodynamics, we find that shocks occur only in a narrow range of parameters. It would be interesting to investigate whether this 'selection effect' operates in radiative hydrodynamics too or if it is a product of the magnetic field.

The power that the shocked cavity can absorb is independent of viscosity and resistivity, as expected. For chromospheric conditions ($\rho_0 \approx 3\ 10^{-9}$ kg m^{-3}, $B_0 \approx 10^{-3}$ T) the Poynting flux provided by Eq. (83) and Fig. 8 is

$$\mathcal{S} \approx 15\epsilon^4 \text{ W m}^{-2}. \tag{89}$$

One competing dissipation mechanism is provided by the release of energy as the cavity 'jumps' from one low–modal, high energy, unstable stationary state to a stable one. Taking into account the limitations of our perturbation scheme, the largest power that can be released in this process is given by Eq. (87) with $R = \epsilon^{-1/2}$, i.e.

$$\mathcal{W} \approx 300\epsilon^{3.5} \text{ W m}^{-2}. \tag{90}$$

For an Alfvén Mach number $\epsilon^3 \approx 10^{-1}$, this figure is about 30 times larger than (89). However we stress that the build-up of

shocks in the cavity, as R is increased, operates in an almost periodic way (see Fig. 7*b*) and that the heating occurs *continuously* at a rate whose time-average is (89). On the other hand, catastrophic transitions depend on the variation of the plasma parameters which are presumably due to *erratic* processes. We envisage that these transitions may possibly account for more sporadic brightenings in the atmosphere.

Acknowledgements. This work was carried out when M. Ruderman was a guest of the Istituto di Fisica Atomica e Molecolare – CNR, Pisa, Italy. We wish to acknowledge the financial support of the Italian National Research Council, which made M. Ruderman's pleasant and fruitful stay in Pisa possible.

References

Bocchialini K., Vial J.-C., Einaudi G., 1997, Statistical Analysis of a Bright Point Observed Simultaneously in Two Chromospheric and Transition Region Lines by SUMER. In: Proceedings of the 5th SOHO workshop 'The Corona and the Solar Wind near Minimum Activity', ESA SP-404, 211

Bologna M., Nocera L., 1998, A&A 336, 735

Braginskii, S.I.: 1965, Transport Processes in Plasma. In: Leontovitch M.A. (ed.) Review of Plasma Physics, Consultants Boureau, New York, vol. 1, 205

Cargill P.J., Spicer D.S., Zalesak S.T., 1997, ApJ 488, 854

Carlsson M., Stein R.F., 1997, ApJ 481, 500

Carlsson M., Judge P.G., Wilhelm K., 1997, ApJ 486, L63

Cheng Q.-Q., Yi Z., 1996, A&A 313, 971

Davila J.M., 1987, ApJ 317, 514

Deubner F.-L., Waldschik Th., Steffen S., 1996, A&A 307, 936

Duvall T.L. Jr., Jefferies S.M., Harvey J.W., et al., 1993, ApJ 410, 829

Foglizzo T., García R.A., Charra J., et al., 1998, A&A 330, 341

Goossens M., 1991, MHD Waves and Wave Heating in non-Uniform Plasmas. In: Priest E.R., Rosner R. (eds.) Advances in Solar System Magnetohydrodynamics, Cambridge Univ. Press, Cambridge, 135

Guckenheimer J., Holmes, P., 1983, Nonlinear oscillations, Dynamical Systems, and Bifurcations of Vector Fields. Springer-Verlag, Berlin

Harvey J.W., Duvall T.L., Jeffries J.W., et al., 1993, Chromospheric Oscillations and the Background Spectrum. In: GONG 1992: Brown T.M. (ed.) Seismic Investigations of the Sun and the Stars, ASP Conference Series, vol. 42, 111

Hoekzema N.M.S., Rutten R.J., 1998, A&A 329, 725

Hofmann J., Steffen S., Deubner F.-L., 1996, A&A 308, 192

Hollweg J.V., 1990, Comput. Phys. Rep. 12, 205

Ionson J.A., 1978, ApJ 226, 650

Judge P., Carlsson M., Wilhelm K., 1997, ApJ 490, L195

Kalkofen W., 1996, ApJ 468, L69

Kalkofen W., 1997, ApJ 486, L145

Kneer F., Hasan S.S., Kalkofen W., 1996, A&A 305, 660

Kneer F., von Uexküll M., 1993, A&A 274, 584

Kuperus M., Ionson J.A., Spicer D., 1981, ARA&A 19, 7

Lites B.W., 1992, Sunspots Oscillations: Observations and Implications. In: Thomas J.H., Weiss N.O. (eds.) Sunspots: Theory and Observations, Kluwer Academic Publishers, Dordrecht, Holland, 261

Lites B.W., Rutten R.J., Kalkofen W., 1993, ApJ 414, 345

Nocera L., 1994, Geophys. Astrophys. Fluid Dynamics 76, 293

Nocera L., Priest E.R., 1991, J. Plasma Phys. 46, 153

Nocera L., Bologna M., Califano F., 1997, Geophys. Astrophys. Fluid Dynamics 86, 131

Ofman L., Davila J.M., Steinolfson R.S., 1994, Geophys. Res. Let. 21, 2259

Ofman L., Davila J.M., 1995, J. Geophys. Res. 100, 23427

Ploner S.R.O., Solanki S.K., 1997, A&A 325, 1199

Press W.H., Teukolsky S.A., Vetterling W.T., et al., 1992, Numerical Recipes in Fortran. The Art of Scientific Computing, Cambridge University Press, Cambridge

Remling B., Deubner F.-L., Steffens S., 1996, A&A 316, 196

Ruderman M.S., Berghmans D., Goossens M., et al., 1997, A&A 320, 305

Schmitz F., Fleck B., 1995, A&A 301, 483

Sivaraman K.R., Livingston W.C., 1982, Solar Phys. 80, 227

Solanki S.K., Steiner O., Uitenbroeck H., 1991, A&A 250, 220

Soltau D., 1997, A&A 317, 586

Steffens S., Deubner F.-L., Hofmann J., et al., 1995, A&A 302, 277

Steffens S., Hofmann J., Deubner F.-L., 1996a, A&A 307, 288

Steffens S., Schmitz F., Deubner F.-L., 1996b, Solar Phys. 172, 85

Stolpe F., Kneer F., 1997, A&A 317, 942

Theurer J., Ulmschneider P., Kalkofen W., 1997, A&A 324, 717

Tirry W.J., Poedts S., 1998, A&A 329, 754

Tu C.-Y., Marsch E., 1997, Solar Phys. 171, 363

Ulmschneider P., Priest E.R., Rosner R. (eds.), 1991, Mechanisms of Chromospheric and Coronal Heating, Springer-Verlag, Berlin

Volkmer R., Kneer F., Bendin C., 1995, A&A 304, L1

von Uexküll M., Kneer F., 1995, A&A 294, 252

Zirin H., Ai G., Wang H. (eds.), 1993, The Magnetic and Velocity Fields of Solar Active Regions, ASP Conference Series, S. Francisco